TWO-DIMENSIONAL DYNAMIC GROUND EFFECT ON A SWIMMING UNDULATING PLATE: A PARAMETRIC STUDY

D. M. Sierra **J. H. Guo***

Engineering Science & Ocean Engineering Department
National Taiwan University
Taipei, Taiwan

ABSTRACT

The dynamic ground effect enhances the swimming of fish. The dynamic ground effect affects the kinematic conditions of fish, causing them to swim more efficiently. However, predicting the degree to which the dynamic ground effect can improve the swimming performance of fish is difficult. The dynamic ground effect can potentially save energy for biomimetic underwater vehicles. Therefore, a theoretical model was developed to investigate the effect of a planar boundary on the swimming performance of a two-dimensional undulating plate. General expressions for the thrust, power input, efficiency, and energy loss of the plate were obtained. As examples, cases in which an undulating plate with linearly varying amplitude swam far from and close to a wall under a range of different kinematic conditions were studied. The dynamic ground effect improved the swimming performance of the plate by reducing the power input while maintaining an almost constant thrust; the degree of improvement depended on the kinematic conditions of the plate. Furthermore, the swimming performance of the plate was improved over a range of distances from the wall; this range of distances also depended on the kinematic conditions of the plate.

Keywords: Undulating plate, Potential flow, Fish swimming, Dynamic ground effect.

1. INTRODUCTION

This work presents a theoretical model of the dynamic ground effect, results obtained using this model agree qualitatively with experimental results presented elsewhere [1, 2]. The ground effect is a widely studied phenomenon, with applications in biology, aerodynamics and hydrodynamics. However, studies of this effect usually involve a rigid body that glides over a solid boundary, such as a rigid airfoil that glides over a wall. But what happens when an undulating body swims near a solid boundary? To properly answer this question, a particular ground effect, called the dynamic ground effect, must be identified; it is the effect that a solid boundary has on the hydrodynamics of an undulating body. This work proposes a simplified theoretical model to study the hydrodynamics of a swimming undulating plate under the dynamic ground effect. Closed-form results are obtained for the thrust and power input coefficients, the efficiency of propulsion and the energy loss of the plate. Theoretical results are obtained for a plate that is swimming with a linear amplitude of undulation.

Several studies of the swimming mechanism of fish with large Reynolds numbers in an unbounded fluid have been published. In these studies, the fluid is considered to be ideal and incompressible, and the body shape of the fish changes with time such that a progressing wave travels down the chord of the fish body in the direction of undisturbed flow. The problem of fish swimming can be understood by applying the general theory of oscillating deformable airfoils. Based on this theory, T. Y. Wu investigated the mechanism of swimming of a two-dimensional flat fish, represented as a two- dimensional plate that moves in a two-dimensional incompressible and inviscid flow. The plate was assumed to be flexible and its thickness was neglected; the efficiency of swimming and the propulsion force of the plate were studied in this two-dimensional regime. T. Y. Wu established the basis of the theory of the swimming of fish in two-dimensional potential flow.

Recently, the situation in which a fish or body is swimming in a bounded fluid, such as close to a planar wall, has been analyzed. Some such studies tackle this problem by considering fish schooling and the swimming of two fish parallel to each other. As an example, E. Kanso and P. K. Newton [3] examined how the swimming mechanism of two fish side by side (which can be regarded as one fish and its image in, a situation analogous to that of a fish and a solid boundary) is affected by

* Corresponding author (jguo@ntu.edu.tw)

DOI : 10.1017/jmech.2017.66
Copyright © 2017 The Society of Theoretical and Applied Mechanics
https://doi.org/10.1017/jmech.2017.66 Published online by Cambridge University Press

their interaction in an inviscid fluid model. The authors argued that the two fish enjoyed locomotory advantages when they were flapping out of phase. B. N. Nowroozi *et al.* carried out an experimental study of swimming fish near a solid boundary [4]. They found that the northern spearnose poacher, *Agonopsis vulsa*, generated forward thrust while overcoming its negative buoyancy by taking advantage of the ground effect when it swam close to the bottom of a water tank. They found that as the fish approached the bottom of the tank, the mechanical efficiency of the pectoral fins increased. E. Blevins and G. V. Lauder conducted experimental studies to analyze the effect of a planar wall on the locomotion of a robotic fin that performed an undulating motion. They found that the ground effect not always increased the swimming efficiency of the undulating fin, but that the ground imposed locomotor penalties on the fin, such that swimming nearer the wall was less efficient. However, they suggested that whether the wall positively or negatively affects the swimming performance of the fin depends on the kinematic conditions of motion. P. W. Webb conducted experiments using real fish and found that a nearby wall improves the swimming performance of fish owing to kinematic changes of the motion of the fish. D. B. Quinn *et al* presented experimental evidence of a positive dynamic ground effect on the hydrodynamic performance of a flexible (non-biological) propulsor. They found that in specific ranges of the flapping frequency, the thrust increased as the propulsor swam closer to the ground.

P. W. Webb reported that fish change their kinematic conditions when swimming near a substrate, such as the ground or a planar wall. However, the range of these kinematic conditions of live fish is difficult to measure owing to the complexity of the motion of their fins. Therefore, understanding the precise relationship between kinematic conditions and the dynamic ground effect, or the impact of the latter on the swimming performance of live fish, is difficult. The ground effect has been widely studied, and the dynamic ground effect has attracted increasing attention in recent years owing to its biological importance and its potential applications in engineering as the basis for reducing the energy consumption of underwater vehicles. The dynamic ground effect has been recently studied experimentally by using man-made flexible swimmers such as undulating fins [1, 5-7], but as has been reported [7], knowledge about the dynamic ground effect is not extensive. Hence, this work proposes a simplified theoretical model of the dynamic ground effect, such that the impact of a boundary on the swimming performance of an undulating two- dimensional plate under various kinematic conditions can be analyzed. Therefore, the difference between this work and similar works that have been published in recent years [1, 3, 5-8] lies in the theoretical model that is developed herein; this model is used to study the dynamic ground effect of an undulating plate using only potential flow with the complex acceleration potential and the image method.

Based on the theory of oscillating airfoils, applied to swimming fish in a two-dimensional potential flow [9, 10], this work develops a model to study the problem of an undulating plate that swims close to a planar wall. This paper comprises eight sections. Section 2 presents the expression for the complex acceleration potential of a plate under the dynamic ground effect. Section 3 concerns the hydrodynamic forces that act on the plate and presents general expressions for power input, thrust and energy loss when the plate is subjected to dynamic ground effect and is swimming with arbitrary varying amplitude. Section 4 presents as example calculations of the swimming performance coefficients of the plate when it is swimming with linearly varying amplitude and is subjected to dynamic ground effect. Section 5 discusses and compares the results in section 4 for a swimming plate with different kinematic conditions, close to and far from a wall. Finally, section 6 presents concluding remarks.

2. COMPLEX ACCELERATION POTENTIAL WITH DYNAMIC GROUND EFFECT

In the following mathematical model all equations are dimensionless. The following characteristic variables are pertinent to the problem to be studied:

- c – characteristic length (the plate's chord)
- U – characteristic velocity (the free stream velocity)
- ω – characteristic frequency (the circular frequency of the plate oscillation)
- τ – characteristic time ($\tau = 2\pi/\omega$)
- σ – reduced frequency of the plate oscillation ($\sigma = \omega c/2U$)

Consider a flat flexible plate with imperceptible thickness from x = -1 to x = 1; the motion of the plate generates the two-dimensional incompressible flow of an inviscid fluid when it is swimming in a uniform flow of constant velocity U in the x–direction. The general form of the flexible plate motion is specified as

$$y = h(x,t), \quad -1 < x < 1, \tag{1}$$

in which $h(x, t)$ is a function of x and time t. The fluid velocity is represented as $\mathbf{q} = (U + u,v)$, in which v and u are the velocities of perturbation in the y- and x- directions respectively, such that the continuity equation is satisfied:

$$\nabla \cdot \mathbf{q} = 0. \tag{2}$$

Under the assumption that v and u are smaller than U, the Euler equations of motion are linearized to yield

$$\left(\frac{\partial}{\partial t} + U\frac{\partial}{\partial x}\right)\mathbf{q} = -\frac{\nabla p}{\rho} = \nabla\Phi, \tag{3}$$

$$\Phi = \frac{(p_\infty - p)}{\rho}. \tag{4}$$

In the above equation p represents the fluid pressure, p_∞ the pressure at infinity (assumed to be constant) and ρ the fluid density. The acceleration potential of Prandtl is denoted as Φ, such that the field of acceleration of the flow is given by $\nabla\Phi$. Therefore, by using the com-

https://doi.org/10.1017/jmech.2017.66 Published online by Cambridge University Press

plex variable $z = x + iy$, the complex acceleration potential can defined as $F(z,t) = \Phi(x,y,t) + i\Psi(x,y,t)$, where $i = \sqrt{-1}$ represents the imaginary unit for the space variables (x,y). The complex velocity is defined as $w(z,t) = u(x,y,t) + iv(x,y,t)$. The linearized Euler equations of motion in (3) are rewritten in terms of $F(z,t)$ and $w(z,t)$ as

$$\frac{\partial F}{\partial z} = \frac{\partial w}{\partial t} + U\frac{\partial w}{\partial z}. \tag{5}$$

To obtain a solution for the complex acceleration potential $F(z,t)$, the boundary conditions are specified [9]. The normal components of the velocity vectors of the fluid and the flexible plate must be equal; the linearized form of this boundary condition is

$$v = \frac{\partial h}{\partial t} + U\frac{\partial h}{\partial x} \quad \text{at} \quad y = \pm 0(-1 < x < 1). \tag{6}$$

A similar boundary condition must exist for the normal components of the acceleration vectors of the fluid and the flexible plate. However an extra limitation must be imposed on the acceleration potential Φ, such that the boundary conditions on velocity and acceleration are both satisfied. Therefore, the complete form of the acceleration boundary condition becomes

$$\frac{\partial \Phi}{\partial y} = a_y = \frac{\partial v}{\partial t} + U\frac{\partial v}{\partial x} = \left(\frac{\partial}{\partial t} + U\frac{\partial}{\partial x}\right)^2 h(x,t) = \frac{D^2 h}{Dt^2}$$
$$\text{at} \quad y = \pm 0, (-1 < x < 1). \tag{7}$$

All over the flow Φ is regular, such that $\Phi(x,0,t) = 0$ for $|x| > 1$ and for all t. The Kutta condition is imposed at the trailing edge of the flexible plate ($z = 1$), such that $|F(1,t)| < \infty$ for all t. Finally, the far field condition is expressed as $F(z,t) \to 0$ as $|z| \to \infty$ and $w(z,t) \to 0$ as $z \to -\infty$. These conditions [9] complete the definition of the problem of the swimming of a flexible plate in a two-dimensional incompressible and inviscid flow in the absence of any solid boundary.

Based on the assumption that harmonic oscillation governs the motion of the plate such that

$$h(x,t) = h_1(x)e^{j\omega t} \text{ for } |x| < 1, \tag{8}$$

where ω is the circular frequency, $h_1(x)$ is a function real in x (and can generally be complex with respect to j), and $j = \sqrt{-1}$ is the imaginary unit for the time variable t, such that $e^{j\omega t} = \cos\omega t + j\sin\omega t$.

For convenience, the conformal transformation $z = 1/2(\zeta + \zeta^{-1})$, which maps the line segment from $x = -1$ to $x = 1$ on the z plane into a circle of unit radius on the ζ plane (such that for the unitary radius circle $\zeta = e^{i\theta}$) is applied, and a new variable is introduced as

$$x = \cos\theta. \tag{9}$$

Expanding $h_1(x)$ in Eq. (8) into a Fourier cosine series [10, 11], yields the motion of the plate in the form

$$h(x,t) = \left[\frac{1}{2}\beta_0 + \sum_{n=1}^{\infty}\beta_n \cos n\theta\right]e^{j\omega t}, \tag{10}$$

with $\beta_n = \frac{2}{\pi}\int_0^{\pi} h_1(x)\cos n\theta d\theta$ for $n = 0,1,2,\ldots$. From Eq. (9) $\partial/\partial x = -(\csc\theta)\partial/\partial\theta$ for $y = 0$ and $|x| < 1$, such that from Eq. (10)

$$\frac{\partial h}{\partial x} = \frac{1}{\sin\theta}\sum_{n=1}^{\infty} n\beta_n \sin n\theta e^{j\omega t} = \left[\frac{\gamma_0}{2} + \sum_{n=1}^{\infty}\gamma_n \cos n\theta\right]e^{j\omega t}, \tag{11}$$

with $\gamma_{n-1} - \gamma_{n+1} = 2n\beta_n$ for $n = 1,2,\ldots$. Solving for the coefficients γ_n and substituting Eqs. (10) and (11) into Eq. (6), yields a Fourier series expression for the velocity boundary condition on the flexible plate as [9, 10]

$$v(x,\pm 0,t) = -U\left[\frac{\lambda_0}{2} + \sum_{n=1}^{\infty}\lambda_n \cos n\theta\right]e^{j\omega t} \quad \text{on} \quad x = \cos\theta, \tag{12}$$

with $\lambda_n = -(\gamma_n + j\sigma\beta_n)$ for $n = 0,1,2,\ldots$, where σ represents the reduced frequency of the plate oscillation, defined as $\sigma = \omega/U$, which is in reference to half of the length of the chord ($c/2$), which in this situation is one.

The complex potential $F(z,t)$ that yields the flow field that is generated by the motion of the oscillating plate in an unbounded fluid and satisfies the above boundary conditions is [9, 10]

$$F(z,t) = \Phi + i\Psi = iU^2\left[\frac{a_0}{\zeta + 1} + \sum_{n=1}^{\infty}\frac{a_n}{\zeta^n}\right]e^{j\omega t} \quad \text{for} \quad |\zeta| > 1, \tag{13}$$

with $\zeta = e^{i\theta}$ on the plate, such that

$$\Phi = U^2\left[\frac{a_0}{2}\tan\frac{\theta}{2} + \sum_{n=1}^{\infty}a_n \sin n\theta\right]e^{j\omega t}, \tag{14}$$

$$\Psi = U^2\left[\frac{a_0}{2} + \sum_{n=1}^{\infty}a_n \cos n\theta\right]e^{j\omega t}, \tag{15}$$

where the coefficients a_n and a_0 are given by the following relations [9]

$$a_n = \lambda_n + \frac{j\sigma}{2n}(\lambda_{n-1} - \lambda_{n+1}) \quad \text{for} \quad n = 1,2,3,\ldots, \tag{16}$$

$$a_0 = (\lambda_0 + \lambda_1)C(\sigma) - \lambda_1. \tag{17}$$

The coefficients a_n (which are real with respect to i) satisfy the regularity condition of Φ, while the coefficient a_0 embodies the leading edge singularity at $\zeta = -1$. The function

$$C(\sigma) = \frac{K_1(j\sigma)}{K_0(j\sigma) + K_1(j\sigma)} = F(\sigma) + jG(\sigma) \tag{18}$$

https://doi.org/10.1017/jmech.2017.66 Published online by Cambridge University Press

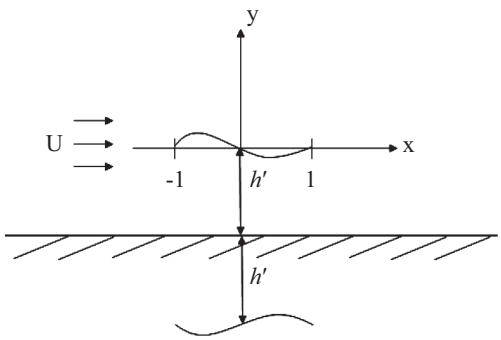


Fig. 1 Swimming flexible plate and its image below planar wall. Plate is located at a distance h' above the wall, with its reflection located at a distance h' below the wall.

is Theodorsen's function [9, 12], whose imaginary and real parts are respectively G and F. K_0 and K_1 represent the modified Bessel functions of the second type. The origin of the complex acceleration potential of a swimming flexible plate of imperceptible thickness in an unbounded two dimensional incompressible and inviscid flow is thus explained [9]. The unbounded complex potential is very important because it is the starting point for determining the bounded complex acceleration potential, which is used to solve the bounded fluid problem, and thereby understand the dynamic ground effect.

Before the complex acceleration potential of the bounded fluid can be found, the physical meaning of the complex acceleration potential in a linear theory must be considered, because the complex acceleration potential is at the core of the solution to the dynamic ground effect problem, and the fact that a linear theory is being used allows a solution to the bounded fluid problem to be found directly from the solution to the unbounded fluid problem by applying the principle of superposition.

The relationship between Prandtl's acceleration potential Φ and the change of pressure, given by Eq. (4), follows from the linearization of the Euler equations of motion. Since the fluid is assumed to be incompressible (ρ = constant) and linearization has been used, Prandtl's acceleration potential Φ becomes directly proportional to the change of pressure in the fluid, according to (4). Therefore, in a linearized theory, the pressure disruption in the flow is directly proportional to the acceleration potential [9], providing a clear physical meaning of the acceleration potential within a linearized theory.

Now, consider the situation in which the undulating plate is swimming next to a plane rigid boundary, which in this case is a horizontal planar wall, as presented in Fig. 1.

This problem can be used to study the swimming of a flat -two-dimensional fish close to a wall, such as a benthic fish (such as a stingray) that swims near the ocean floor. The Reynolds numbers of such fish are of the order of $O(10^4)$ [1], so thin boundary layers develop around their bodies. By representing this kind of flat fish as a flexible flat plate of negligible thickness, the displacement thickness of the boundary layer can be found as a function of the chord length of the plate. The displacement thickness of the boundary layer for a flat plate in a uniform flow can be calculated as

$$\delta^* = 1.7208\left(c/\sqrt{\mathrm{Re}_c}\right) = 1.7208\left(c/\sqrt{10^4}\right) = 1.72080\times10^{-2}c$$

[13], where c represents the chord of the plate (which is one body length). Therefore, to study the dynamic ground effect, the potential flow method can be used when the minimum distance $h'_{\min}$ between the plate and the wall is one order of magnitude larger than δ^*, such that $h'_{\min} \geq 1\times10^{-1}c$.

Since the unbounded fluid acceleration potential of an undulating plate, given by Eq. (14), is obtained using a linearized theory [9, 10], the case of an undulating plate and a planar wall can be analyzed by using the superposition principle. Therefore, the bounded fluid problem can be solved using the image method, by replacing the wall with an image plate (a reflection of the plate through the wall), symmetrically on the opposite side of the wall at a distance h' and with symmetric motion, such that the boundary condition on the wall $\partial\Phi/\partial y = 0$ is satisfied. In this sense, the plate-wall interactions can be regarded as the interactions between the two identical and adjacent plates. In this case, from Eq. (13), the complex acceleration potential for the image body takes the form

$$\begin{aligned}\overline{F(z,t)} &= \overline{\Phi} - i\overline{\Psi} \\ &= -iU^2\left[\frac{\overline{a_0}}{\overline{\zeta}+1+2ih'} + \sum_{n=1}^{\infty}\frac{\overline{a_n}}{\left(\overline{\zeta}+2ih'\right)^n}\right]e^{-j\omega t} \quad \text{for } |\zeta|>1,\end{aligned} \tag{19}$$

with

$$\overline{\Phi} = U^2\left\{\begin{array}{l}\dfrac{\overline{a_0}\sin\theta - 2\overline{a_0}h'}{(1+\cos\theta)^2+(2h'-\sin\theta)^2} \\ +\mathrm{Re}\left[\displaystyle\sum_{n=1}^{\infty}\frac{-i\overline{a_n}}{\left(e^{-i\theta}+2ih'\right)^n}\right]\end{array}\right\}e^{-j\omega t}, \tag{20}$$

$$\overline{\Psi} = U^2\left\{\begin{array}{l}\dfrac{\overline{a_0}+\overline{a_0}\cos\theta}{(1+\cos\theta)^2+(2h'-\sin\theta)^2} \\ -\mathrm{Im}\left[\displaystyle\sum_{n=1}^{\infty}\frac{-i\overline{a_n}}{\left(e^{-i\theta}+2ih'\right)^n}\right]\end{array}\right\}e^{-j\omega t}, \tag{21}$$

where the coefficients $\overline{a_n}$ and $\overline{a_0}$ are the complex conjugated values of (16) and (17) respectively, and are expressed as

$$\overline{a_n} = \overline{\lambda_n} - \frac{j\sigma}{2n}\left(\overline{\lambda_{n-1}} - \overline{\lambda_{n+1}}\right) \quad \text{for} \quad n=1,2,3,..., \tag{22}$$

$$\overline{a_0} = \left(\overline{\lambda_0}+\overline{\lambda_1}\right)\overline{C(\sigma)} - \overline{\lambda_1}, \tag{23}$$

https://doi.org/10.1017/jmech.2017.66 Published online by Cambridge University Press

where $\overline{\lambda_n} = -\left(\overline{\gamma_n} - j\sigma\overline{\beta_n}\right)$ and $\overline{C(\sigma)} = F(\sigma) - jG(\sigma)$. Since this analysis is within the framework of a linearized theory, applying the superposition principle yields the complex acceleration potential of the flexible plate and its image as

$$F_{Total}(z,t) = iU^2\left[\frac{a_0}{\zeta+1} + \sum_{n=1}^{\infty}\frac{a_n}{\zeta^n}\right]e^{j\omega t} - iU^2\left[\frac{\overline{a_0}}{\overline{\zeta}+1+2ih'} + \sum_{n=1}^{\infty}\frac{\overline{a_n}}{\left(\overline{\zeta}+2ih'\right)^n}\right]e^{-j\omega t}. \tag{24}$$

The above expression represents the total complex acceleration potential that is associated with the two-dimensional dynamic ground effect of a swimming flexible plate. This is the core of the solution to the bounded fluid problem.

3. HYDRODYNAMIC FORCES, POWER REQUIRED AND ENERGY LOSS

Applying the superposition principle according to (4), (14) and (20), yields the difference in the pressure across the plate when the plate is next to a planar wall as

$$(\Delta p) = \rho U^2\left\{\left[a_0\tan\frac{\theta}{2} + 2\sum_{n=1}^{\infty}a_n\sin n\theta\right]e^{j\omega t} + \left[\frac{2\overline{a_0}\sin\theta - 4\overline{a_0}h'}{(1+\cos\theta)^2 + (2h'-\sin\theta)^2} + 2\,\mathrm{Re}\left[\sum_{n=1}^{\infty}\frac{-i\overline{a_n}}{\left(e^{-i\theta}+2ih'\right)^n}\right]\right]e^{-j\omega t}\right\}, \tag{25}$$

where Δp is positive in the positive y-direction. Splitting the pressure into its imaginary and real parts is helpful, as is done here using the following definitions [10]. For $n = 0,1,2,...,$

$$\begin{aligned}&\beta_n e^{j\omega t} = B_n' + jB_n'', \quad \gamma_n e^{j\omega t} = \Gamma_n' + j\Gamma_n'', \quad a_n e^{j\omega t} = A_n' + jA_n'', \quad \lambda_n e^{j\omega t} = \Lambda_n' + j\Lambda_n'',\\ &\overline{\beta_n} e^{-j\omega t} = \overline{B_n'} - j\overline{B_n''}, \quad \overline{\gamma_n} e^{-j\omega t} = \overline{\Gamma_n'} - j\overline{\Gamma_n''}, \quad \overline{a_n} e^{-j\omega t} = \overline{A_n'} - j\overline{A_n''}, \quad \overline{\lambda_n} e^{-j\omega t} = \overline{\Lambda_n'} - j\overline{\Lambda_n''}\end{aligned} \tag{26}$$

such that

$$(\Delta p)_R = \rho U^2\left\{A_0'\tan\frac{\theta}{2} + 2\sum_{n=1}^{\infty}A_n'\sin n\theta + \frac{2\overline{A_0'}\sin\theta - 4\overline{A_0'}h'}{(1+\cos\theta)^2 + (2h'-\sin\theta)^2} + 2\,\mathrm{Re}\left[\sum_{n=1}^{\infty}\frac{-i\overline{A_n'}}{\left(e^{-i\theta}+2ih'\right)^n}\right]\right\}, \tag{27}$$

where the R subscript indicates the real part of (Δp) with respect to j.

The lift is given by

$$L = \int_{-1}^{1}(\Delta p)\,dx = \rho U^2\left\{\pi(a_0+a_1)e^{j\omega t} + \left[\frac{\overline{a_0}}{\left(1+4h'^2\right)^2}\Theta_1 - \frac{2\overline{a_0}}{1+4h'^2}\Theta_2 - \overline{a_1}\left(\frac{2+3h'(8h'+\pi)}{12h'^3}\right)\right]e^{-j\omega t}\right\}, \tag{28}$$

with

$$\begin{aligned}\Theta_1 &\equiv \left[3\pi - 4h'\left(1+4h'^2-\pi h'\right) + 4\left(1+3h'^2+4h'^4\right)\cot^{-1}h' - 4h'\left(1+2h'^2\right)\left(\ln h'^2 - \ln\left(1+h'^2\right)\right)\right],\\ \Theta_2 &\equiv \left[\pi + \left(2+4h'^2\right)\cot^{-1}h' - h'\ln h'^2 + h'\ln\left(1+h'^2\right)\right].\end{aligned} \tag{29}$$

The real part of Eq. (28) with respect to j yields

$$L_R = \rho U^2\left\{\pi\left(A_0'+A_1'\right) + \frac{\overline{A_0'}}{\left(1+4h'^2\right)^2}\Theta_1 - \frac{2\overline{A_0'}}{1+4h'^2}\Theta_2 - \overline{A_1'}\left(\frac{2+3h'(8h'+\pi)}{12h'^3}\right)\right\}. \tag{30}$$

The thrust (including the thrust on the plate and the thrust due to leading edge suction) is calculated as

$$T = \int_{-1}^{1}(\Delta p)_R\left(\frac{\partial h}{\partial x}\right)_R dx + T_S, \tag{31}$$

where, from Eq. (11),

https://doi.org/10.1017/jmech.2017.66 Published online by Cambridge University Press

$$\left(\frac{\partial h}{\partial x}\right)_R = \left[\frac{\Gamma_0'}{2} + \sum_{m=1}^{\infty} \Gamma_m' \cos m\theta\right]. \tag{32}$$

Substituting $\gamma_{n-1} - \gamma_{n+1} = 2n\beta_n$, $\lambda_n = -\left(\gamma_n + j\sigma\beta_n\right)$, (16), $\overline{\gamma_{n-1}} - \overline{\gamma_{n+1}} = 2n\overline{\beta_n}$, $\overline{\lambda_n} = -\left(\overline{\gamma_n} - j\sigma\overline{\beta_n}\right)$ and Eq. (22) into Eq. (26), yields following relations after some manipulation.

$$\begin{aligned}
&\Gamma_{n-1}'' - \Gamma_{n+1}'' = 2nB_n'', \quad \Gamma_{n-1}' - \Gamma_{n+1}' = 2nB_n', \quad A_n' = \left(\sigma^2/2n\right)\left(B_{n-1}' - B_{n+1}'\right) + 2\sigma B_n'' - \Gamma_n', \\
&\overline{\Gamma_{n-1}''} - \overline{\Gamma_{n+1}''} = 2n\overline{B_n''}, \quad \overline{\Gamma_{n-1}'} - \overline{\Gamma_{n+1}'} = 2n\overline{B_n'}, \quad \overline{A_n'} = \left(\sigma^2/2n\right)\left(\overline{B_{n-1}'} - \overline{B_{n+1}'}\right) + 2\sigma\overline{B_n''} - \overline{\Gamma_n'};
\end{aligned} \tag{33}$$

with $n = 0,1,2,\ldots$. Similarly, from the previous definitions of λ_n and $\overline{\lambda_n}$, as well as from Eq. (26), the following relations are obtained for $n = 0,1,2,\ldots$.

$$\Lambda_n' = \sigma B_n'' - \Gamma_n', \quad \Lambda_n'' = -\left(\sigma B_n' + \Gamma_n''\right), \quad \overline{\Lambda_n'} = \sigma\overline{B_n''} - \overline{\Gamma_n'}, \quad \overline{\Lambda_n''} = -\left(\sigma\overline{B_n'} + \overline{\Gamma_n''}\right). \tag{34}$$

Directly substituting Eqs. (32) and (27) into Eq. (31), and eliminating A_n' and $\overline{A_n'}$ using Eq. (33), yields the thrust as

$$\begin{aligned}
T = \frac{1}{2}\pi\rho U^2 \Bigg[&\left(A_0' + \Gamma_0'\right)\left(A_0' - \Gamma_1'\right) + \sigma^2 B_0' B_1' + 4\sigma\sum_{n=1}^{\infty} nB_n' B_n'' + \overline{A_0'}\left(\overline{\Gamma_1'}H_1 - \overline{\Gamma_0'}H_2\right) - \overline{\Gamma_1'}\,\overline{\Gamma_0'}H_3 + \sigma^2\overline{B_0'}\,\overline{\Gamma_0'}\frac{H_3}{2} \\
&+ 2\sigma\sum_{n=1}^{\infty}\overline{B_n''}\left(\overline{\Gamma_0'}H_{5n} + \overline{\Gamma_1'}H_{6n}\right)\Bigg]
\end{aligned} \tag{35}$$

with

$$\begin{aligned}
H_1 &\equiv \frac{1}{\pi\left(1+4h'^2\right)^3}\Bigg[4h'\left(2+8h'^2+3h'\pi\right) - \pi + 8h'^2\left(3+6h'^2+8h'^4\right)\tan^{-1}\left(\frac{1}{h'}\right) \\
&\quad + 4h'\left(1+2\left[h'^2+6h'^4+8h'^6\right]\right)\left(\ln h'^2 - \ln\left(1+h'^2\right)\right)\Bigg], \\
H_2 &\equiv \frac{1}{\pi\left(1+4h'^2\right)^2}\left[4h'\left(1+h'\left[4h'+\pi\right]\right) - \pi + 2h'\left(2h'\left[3+4h'^2\right]\tan^{-1}\left(\frac{1}{h'}\right) + \ln h'^2 - \ln\left(1+h'^2\right)\right)\right], \\
H_3 &\equiv \frac{24h'^2 - 3\pi h' - 2}{12\pi h'^3}, \\
H_{5n} &\equiv \frac{2}{\pi}\mathrm{Re}\left[-\frac{1}{3}\frac{i}{\left(2h'\right)^{n+2}}\left(24h'^2 e^{i\pi n/2} + e^{-i\pi n/2}\left[3h'\pi n + n^2 + n\right]\right)\right], \\
H_{6n} &\equiv \frac{2}{\pi}\mathrm{Re}\left[\frac{1}{15}\frac{e^{-i\pi n/2}n}{2^{n+4}h'^{n+3}}\left(160h'^2 + 15\pi h'\left[n+1\right] + 4n^2 + 12n + 8\right)\right].
\end{aligned} \tag{36}$$

The power that is needed for the plate to keep moving is defined as the work executed over time by an external force. This applied external force must be opposite and equal to the corresponding force owing to the pressure that acts across the plate. Therefore, the power input is

$$P = -\int_{-1}^{1}\left(\Delta p\right)_R\left(\frac{\partial h}{\partial t}\right)_R dx, \tag{37}$$

with

$$\left(\frac{\partial h}{\partial t}\right)_R = -\omega\left[\frac{1}{2}B_0'' + \sum_{m=1}^{\infty} B_m'' \cos m\theta\right]. \tag{38}$$

A manipulation similar to that performed to obtain the thrust yields the power input for maintaining the motion as

https://doi.org/10.1017/jmech.2017.66 Published online by Cambridge University Press

$$P=\frac{1}{2}\pi\rho U^3\sigma\Big[A_0'\left(B_0''-B_1''\right)+2\sigma B_0''B_1''-B_0''\Gamma_1'-B_1''\Gamma_0'+2\sum_{n=1}^{\infty}nB_n'B_n''+\sigma^2\sum_{n=1}^{\infty}\frac{1}{2n}\left(B_{n-1}'-B_{n+1}'\right)\left(B_{n-1}''-B_{n+1}''\right)$$
$$+\overline{A_0'}\left(\overline{B_1''}H_1-\overline{B_0''}H_2\right)+2\sigma\overline{B_1''}\,\overline{B_0''}H_3-\overline{\Gamma_1'}\,\overline{B_0''}H_3-\overline{B_1''}\,\overline{\Gamma_0'}H_4+2\sum_{n=1}^{\infty}n\overline{B_n'}\,\overline{B_n''}H_4$$
$$+\sigma^2\sum_{n=1}^{\infty}\frac{1}{2n}\left(\overline{B_{n-1}'}-\overline{B_{n+1}'}\right)\left(\overline{B_0''}H_{5n}+\overline{B_1''}H_{6n}\right)\Big] \tag{39}$$

with

$$H_4\equiv\frac{2}{\pi h'}. \tag{40}$$

The kinetic energy that is conveyed into the flow is obtained using the principle of the conservation of energy

$$E_W=P-TU. \tag{41}$$

A straightforward substitution of Eqs. (35) and (39) into Eq. (41), and subsequent manipulation using the relations given in (34), yield the energy lost into the fluid as,

$$E_W=\frac{1}{2}\pi\rho U^3\Bigg[\left(\Lambda_0-A_0'\right)\left(\Lambda_1'+A_0'\right)-\sigma\sum_{n=1}^{\infty}\frac{1}{2n}\left(\Lambda_{n-1}'-\Lambda_{n+1}'\right)\left(\Lambda_{n-1}''-\Lambda_{n+1}''\right)+\overline{A_0'}\left(\overline{\Lambda_1'}H_1-\overline{\Lambda_0'}H_2\right)-\overline{\Gamma_1'}\,\overline{\Lambda_0'}H_3$$
$$-\overline{\Gamma_0'}\left(\overline{\Lambda_1'}+\overline{\Gamma_1'}\right)H_4+\sigma^2\overline{B_1''}\,\overline{B_0''}H_3-\sigma\overline{B_1''}\,\overline{\Gamma_0'}H_3+2\sigma\sum_{n=1}^{\infty}n\overline{B_n'}\,\overline{B_n''}H_4-\sigma\sum_{n=1}^{\infty}\frac{1}{2n}\left(\overline{\Lambda_{n-1}''}-\overline{\Lambda_{n+1}''}\right)\left(\overline{\Lambda_0'}H_{5n}+\overline{\Lambda_1'}H_{6n}\right)\Bigg]. \tag{42}$$

The averaged power input and thrust in one period of oscillation of undulation of the plate, given by $\tau=2\pi/\omega$, can be obtained, and used to calculate the propulsive efficiency for a single period of oscillation of the plate. Using the definition of the time average of an arbitrary time function $g(t)$ given by $\langle g(t)\rangle=\frac{1}{\tau}\int_0^{\tau}g(t)\,dt$, the average values of Eqs. (35), (39) and (42) can be obtained by separating the following expressions into the real and imaginary parts

$$\beta_n=\beta_n'+j\beta_n'',\quad \overline{\beta_n}=\beta_n'-j\beta_n'' \tag{43}$$

for $n=0,1,2,\ldots$, with β_n' and β_n'' as the real and imaginary parts of β_n and $\overline{\beta_n}$, respectively. Therefore, from Eq. (26),

$$B_n'=\beta_n'\cos\omega t-\beta_n''\sin\omega t,\ B_n''=\beta_n''\cos\omega t+\beta_n'\sin\omega t,\ \overline{B_n'}=\beta_n'\cos\omega t-\beta_n''\sin\omega t,\ \overline{B_n''}=\beta_n''\cos\omega t+\beta_n'\sin\omega t. \tag{44}$$

Similarly, the following expressions are obtained.

$$\Gamma_n'=\gamma_n'\cos\omega t-\gamma_n''\sin\omega t,\ \Gamma_n''=\gamma_n'\sin\omega t+\gamma_n''\cos\omega t,\ \Lambda_n'=\lambda_n'\cos\omega t-\lambda_n''\sin\omega t,\ \Lambda_n''=\lambda_n'\sin\omega t+\lambda_n''\cos\omega t,$$
$$\overline{\Gamma_n'}=\gamma_n'\cos\omega t-\gamma_n''\sin\omega t,\ \overline{\Gamma_n''}=\gamma_n'\sin\omega t+\gamma_n''\cos\omega t,\ \overline{\Lambda_n'}=\overline{\lambda_n'}\cos\omega t-\overline{\lambda_n''}\sin\omega t,\ \overline{\Lambda_n''}=\overline{\lambda_n'}\sin\omega t+\overline{\lambda_n''}\cos\omega t. \tag{45}$$

The equations

$$\langle\cos^2\omega t\rangle=\langle\sin^2\omega t\rangle=\frac{1}{2},\ \text{and}\ \langle\sin\omega t\cos\omega t\rangle=0, \tag{46}$$

yields the average values over time of the thrust, power input and kinetic energy loss as

$$\langle T\rangle=\frac{1}{2}\pi\rho U^2\left\langle\left(A_0'+\Gamma_0'\right)\left(A_0'-\Gamma_1'\right)+\sigma^2B_0'B_1'+\overline{A_0'}\left(\overline{\Gamma_1'}H_1-\overline{\Gamma_0'}H_2\right)-\overline{\Gamma_1'}\,\overline{\Gamma_0'}H_3+\sigma^2\overline{B_0'}\,\overline{\Gamma_0'}\frac{H_3}{2}+2\sigma\overline{B_1''}\,\overline{\Gamma_0'}H_3\right\rangle, \tag{47}$$

$$\langle P\rangle=\frac{1}{2}\pi\rho U^3\sigma\left\langle A_0'\left(B_0''-B_1''\right)+2\sigma B_0''B_1''-B_0''\Gamma_1'-B_1''\Gamma_0'+\overline{A_0'}\left(\overline{B_1''}H_1-\overline{B_0''}H_2\right)+2\sigma\overline{B_1''}\,\overline{B_0''}H_3-\overline{\Gamma_1'}\,\overline{B_0''}H_3-\overline{B_1''}\,\overline{\Gamma_0'}H_4\right\rangle, \tag{48}$$

$$\langle E_W\rangle=\frac{1}{2}\pi\rho U^3\left\langle\left(\Lambda_0'-A_0'\right)\left(\Lambda_1'+A_0'\right)+\overline{A_0'}\left(\overline{\Lambda_1'}H_1-\overline{\Lambda_0'}H_2\right)-\overline{\Gamma_1'}\,\overline{\Lambda_0'}H_3-\left(\overline{\Lambda_1'}+\overline{\Gamma_1'}\right)\overline{\Gamma_0'}H_4+\sigma^2\overline{B_1''}\,\overline{B_0''}H_3-\sigma\overline{B_1''}\,\overline{\Gamma_0'}H_3\right\rangle$$
$$=\frac{1}{4}\pi\rho U^3\Big\{\Big[\left(\lambda_0'+\lambda_1'\right)^2+\left(\lambda_0''+\lambda_1''\right)^2\Big]\Big[F-\left(F^2+G^2\right)\Big]+\Big[H_1\left(\overline{\lambda_0'}\lambda_1''-\overline{\lambda_0''}\lambda_1'\right)+H_2\left(\overline{\lambda_1''}\lambda_0'-\overline{\lambda_1'}\lambda_0''\right)\Big]G-H_1\left(\overline{\lambda_1'}^2+\overline{\lambda_1''}^2\right)$$
$$+\Big[H_1\left(\overline{\lambda_0'}\lambda_1'+\overline{\lambda_0''}\lambda_1''+\overline{\lambda_1'}^2+\overline{\lambda_1''}^2\right)-H_2\left(\overline{\lambda_1'}\lambda_0'+\overline{\lambda_1''}\lambda_0''+\overline{\lambda_0'}^2+\overline{\lambda_0''}^2\right)\Big]F+H_2\left(\overline{\lambda_1'}\lambda_0'+\overline{\lambda_1''}\lambda_0''\right)-H_3\left(\gamma_1'\overline{\lambda_0'}+\gamma_1''\overline{\lambda_0''}\right)$$
$$-H_4\left(\overline{\lambda_1'}\gamma_0'+\overline{\lambda_1''}\gamma_0''+\gamma_1'\gamma_0'+\gamma_1''\gamma_0''\right)+\sigma^2H_3\left(\beta_1'\beta_0'+\beta_1''\beta_0''\right)-\sigma H_3\left(\beta_1''\gamma_0'-\beta_1'\gamma_0''\right)\Big\}, \tag{49}$$

https://doi.org/10.1017/jmech.2017.66 Published online by Cambridge University Press

where the final form of $\langle E_W \rangle$ in Eq. (49) was obtained using the definitions $A_0' = (\Lambda_0' + \Lambda_1')F(\sigma) - (\Lambda_0'' + \Lambda_1'')G(\sigma) - \Lambda_1'$, $\overline{A_0'} = (\overline{\Lambda_0'} + \overline{\Lambda_1'})F(\sigma) - (\overline{\Lambda''_0} + \overline{\Lambda''_1})G(\sigma) - \overline{\Lambda_1'}$ [10], and Eqs. (45) and (46). Equations (47), (48) and (49) respectively represent the time average values of thrust, power input and energy loss of a swimming plate with harmonic oscillation under the dynamic ground effect; these equations are in their general form.

Equations (47), (48) and (49) concern the situation in which the plate is swimming with arbitrary varying amplitude. First, consider the motion of the plate that exhibits a train of progressive waves of arbitrary varying amplitude, frequency $\omega/2\pi$ and wavelength $\lambda = 2\pi/k$. The motion of such a plate satisfies the following;

$$h(x,t) = \left[\sum_{m=0}^{\infty} b_m x^m e^{j\varepsilon_m}\right] e^{j(\omega t - kx)} = \sum_{m=0}^{\infty} b_m j^m \left(\frac{\partial}{\partial k}\right)^m e^{j(\omega t - kx + \varepsilon_m)}$$
$$= \sum_{m=0}^{\infty} b_m j^m e^{j\varepsilon_m} \left[J_0^{(m)}(k) + 2\sum_{n=1}^{\infty}(-j)^n J_n^{(m)}(k)\cos n\theta\right] e^{j\omega t} \tag{50}$$

in which the last part is obtained using $e^{-jkx} = e^{-jk\cos\theta} = J_0(k) + 2\sum_{n=1}^{\infty}(-j)^n J_n(k)\cos n\theta$. The amplitude of the wave is assumed to be a function of x (expressed in terms of a series); the coefficients b_m are real, and ε_m are constant phase angles. The function $J_n(k)$ is the Bessel function of the first kind, with $J_n^{(m)}(k) = d^m J_n(k)/dk^m$ [10].

To obtain expressions for $\langle T \rangle$, $\langle P \rangle$ and $\langle E_W \rangle$ when the plate exhibits harmonic motion with arbitrary varying amplitude, the following procedure is performed. The differential operators D_{I} and D_{II} defined in reference [10] are used.

$$D_{\mathrm{I}}(m,t) = (-)^m \left[b_{2m}\cos(\omega t + \varepsilon_{2m})\left(\frac{\partial}{\partial k}\right)^{2m} - b_{2m+1}\sin(\omega t + \varepsilon_{2m+1})\left(\frac{\partial}{\partial k}\right)^{2m+1}\right],$$
$$D_{\mathrm{II}}(m,t) = (-)^m \left[b_{2m}\sin(\omega t + \varepsilon_{2m})\left(\frac{\partial}{\partial k}\right)^{2m} + b_{2m+1}\cos(\omega t + \varepsilon_{2m+1})\left(\frac{\partial}{\partial k}\right)^{2m+1}\right]. \tag{51}$$

The coefficients that appear in Eqs. (47) and (48) are given by

$$B_{2n}' = 2(-)^n \sum_{m=0}^{\infty} D_{\mathrm{I}}(m,t) J_{2n}(k),\ B_{2n+1}'' = -2(-)^n \sum_{m=0}^{\infty} D_{\mathrm{I}}(m,t) J_{2n+1}(k),\ B_{2n}'' = 2(-)^n \sum_{m=0}^{\infty} D_{\mathrm{II}}(m,t) J_{2n}(k),$$
$$B_{2n+1}' = 2(-)^n \sum_{m=0}^{\infty} D_{\mathrm{II}}(m,t) J_{2n+1}(k),\ \Gamma_{2n}' = 2(-)^n \sum_{m=0}^{\infty} D_{\mathrm{II}}(m,t) k J_{2n}(k),\ \Gamma_{2n+1}'' = -2(-)^n \sum_{m=0}^{\infty} D_{\mathrm{II}}(m,t) k J_{2n+1}(k),$$
$$\Gamma_{2n}'' = -2(-)^n \sum_{m=0}^{\infty} D_{\mathrm{I}}(m,t) k J_{2n}(k),\ \Gamma_{2n+1}' = -2(-)^n \sum_{m=0}^{\infty} D_{\mathrm{I}}(m,t) k J_{2n+1}(k),$$
$$A_0' = 2\sum_{m=0}^{\infty}\left[D_{\mathrm{II}}(m,t)\Omega(\sigma,k) + D_{\mathrm{I}}(m,t)Q(\sigma,k)\right], \tag{52}$$

with $n = 0,1,2,\ldots$ and

$$\Omega(\sigma,k) \equiv (\sigma - k)\left[F(\sigma)J_0(k) + G(\sigma)J_1(k)\right],\ Q(\sigma,k) \equiv (\sigma - k)\left[(1 - F(\sigma))J_1(k) + G(\sigma)J_0(k)\right]. \tag{53}$$

From Eqs. (44), (45) and (52), expressions for the coefficients $\overline{B_{2n}'}$, $\overline{B_{2n+1}'}$, $\overline{B_{2n}''}$, $\overline{B_{2n+1}''}$, $\overline{\Gamma_{2n}'}$, $\overline{\Gamma_{2n+1}'}$, $\overline{\Gamma_{2n}''}$ and $\overline{\Gamma_{2n+1}''}$ are

$$\overline{B_{2n}'} = B_{2n}',\ \overline{B_{2n+1}'} = B_{2n+1}',\ \overline{B_{2n}''} = B_{2n}'',\ \overline{B_{2n+1}''} = B_{2n+1}'',\ \overline{\Gamma_{2n}'} = \Gamma_{2n}',\ \overline{\Gamma_{2n+1}'} = \Gamma_{2n+1}',\ \overline{\Gamma_{2n}''} = \Gamma_{2n}'',\ \overline{\Gamma_{2n+1}''} = \Gamma_{2n+1}'',\ \overline{A_0'} = A_0'. \tag{54}$$

The coefficients λ_m', λ_m'', $\overline{\lambda_m'}$ and $\overline{\lambda_m''}$ (for $m = 0$, 1) in Eq. (49) are given by [10]

$$\lambda_0' = 2\sum_{m=0}^{\infty} D_{\mathrm{II}}(m,0)(\sigma - k)J_0(k),\ \lambda_1'' = -2\sum_{m=0}^{\infty} D_{\mathrm{II}}(m,0)(\sigma - k)J_1(k),\ \lambda_0'' = -2\sum_{m=0}^{\infty} D_{\mathrm{I}}(m,0)(\sigma - k)J_0(k),$$
$$\lambda_1' = -2\sum_{m=0}^{\infty} D_{\mathrm{I}}(m,0)(\sigma - k)J_1(k),\ \overline{\lambda_0'} = 2\sum_{m=0}^{\infty} D_{\mathrm{II}}(m,0)(\sigma - k)J_0(k),\ \overline{\lambda_0''} = 2\sum_{m=0}^{\infty} D_{\mathrm{I}}(m,0)(\sigma - k)J_0(k),$$
$$\overline{\lambda_1'} = -2\sum_{m=0}^{\infty} D_{\mathrm{I}}(m,0)(\sigma - k)J_1(k),\ \overline{\lambda_1''} = 2\sum_{m=0}^{\infty} D_{\mathrm{II}}(m,0)(\sigma - k)J_1(k). \tag{55}$$

https://doi.org/10.1017/jmech.2017.66 Published online by Cambridge University Press

The average thrust coefficient is obtained from a straightforward substitution of Eqs. (52) and (54) into Eq. (47) to yield

$$\begin{aligned}\frac{\langle T\rangle}{\pi\rho U^2}=&-4\sigma\left\langle\sum_{m=0}^{\infty}\sum_{r=0}^{\infty}\left[D_{\mathrm{I}}(m,t)J_1(k)\right]\left[D_{\mathrm{II}}(r,t)kJ_0(k)\right]\right\rangle H_3+2\sigma^2\left\langle\sum_{m=0}^{\infty}\sum_{r=0}^{\infty}\left[D_{\mathrm{I}}(m,t)J_0(k)\right]\left[D_{\mathrm{II}}(r,t)J_1(k)\right]\right\rangle\\&-2\left\langle\sum_{m=0}^{\infty}\sum_{r=0}^{\infty}\left[D_{\mathrm{II}}(m,t)\Omega\right]\left[D_{\mathrm{I}}(r,t)kJ_1(k)\right]\right\rangle H_1-2\left\langle\sum_{m=0}^{\infty}\sum_{r=0}^{\infty}\left[D_{\mathrm{I}}(m,t)Q\right]\left[D_{\mathrm{I}}(r,t)kJ_1(k)\right]\right\rangle H_1\\&-2\left\langle\sum_{m=0}^{\infty}\sum_{r=0}^{\infty}\left[D_{\mathrm{II}}(m,t)\Omega\right]\left[D_{\mathrm{II}}(r,t)kJ_0(k)\right]\right\rangle H_2-2\left\langle\sum_{m=0}^{\infty}\sum_{r=0}^{\infty}\left[D_{\mathrm{I}}(m,t)Q\right]\left[D_{\mathrm{II}}(r,t)kJ_0(k)\right]\right\rangle H_2\\&+2\left\langle\sum_{m=0}^{\infty}\sum_{r=0}^{\infty}\left[D_{\mathrm{I}}(m,t)kJ_1(k)\right]\left[D_{\mathrm{II}}(r,t)kJ_0(k)\right]\right\rangle H_3+\sigma^2\left\langle\sum_{m=0}^{\infty}\sum_{r=0}^{\infty}\left[D_{\mathrm{I}}(m,t)J_0(k)\right]\left[D_{\mathrm{II}}(r,t)kJ_0(k)\right]\right\rangle H_3\\&+2\left\langle\sum_{m=0}^{\infty}\sum_{r=0}^{\infty}\left[D_{\mathrm{II}}(m,t)\Omega_*+D_{\mathrm{I}}(m,t)Q\right]\left[D_{\mathrm{II}}(r,t)\Omega+D_{\mathrm{I}}(r,t)Q_*\right]\right\rangle\end{aligned}\tag{56}$$

with Q_* and Ω_* defined [10] as

$$\Omega_*=\Omega(\sigma,k)+kJ_0(k),\ \ Q_*=Q(\sigma,k)+kJ_1(k).\tag{57}$$

In a manner similar to that used to obtain Eq. (56), Eqs. (34), (54), and (55) are substituted into Eq. (49) to yield the average energy loss coefficient as

$$\begin{aligned}\frac{\langle E_W\rangle}{\pi\rho U^3}=&\frac{1}{4}\Bigg\{H_1\left(\left[-2\sum_{m=0}^{\infty}D_I(m,0)N_1(\sigma,k)\right]^2+\left[2\sum_{m=0}^{\infty}D_{II}(m,0)N_1(\sigma,k)\right]^2\right)F\\&-4H_1\left(\left[\sum_{m=0}^{\infty}D_{\mathrm{II}}(m,0)N_0(\sigma,k)\right]\left[\sum_{m=0}^{\infty}D_{\mathrm{I}}(m,0)N_1(\sigma,k)\right]-\left[\sum_{m=0}^{\infty}D_{\mathrm{I}}(m,0)N_0(\sigma,k)\right]\left[\sum_{m=0}^{\infty}D_{\mathrm{II}}(m,0)N_1(\sigma,k)\right]\right)F\\&+\left[\left(2\sum_{m=0}^{\infty}D_{\mathrm{II}}(m,0)N_0(\sigma,k)-2\sum_{m=0}^{\infty}D_{\mathrm{I}}(m,0)N_1(\sigma,k)\right)^2+\left(-2\sum_{m=0}^{\infty}D_{\mathrm{I}}(m,0)N_0(\sigma,k)-2\sum_{m=0}^{\infty}D_{\mathrm{II}}(m,0)N_1(\sigma,k)\right)^2\right]\\&\left[F-\left(F^2+G^2\right)\right]+4H_2\left(\left[\sum_{m=0}^{\infty}D_{\mathrm{I}}(m,0)N_1(\sigma,k)\right]\left[\sum_{m=0}^{\infty}D_{\mathrm{II}}(m,0)N_0(\sigma,k)\right]-\left[\sum_{m=0}^{\infty}D_{\mathrm{II}}(m,0)N_1(\sigma,k)\right]\right.\\&\left.\left[\sum_{m=0}^{\infty}D_{\mathrm{I}}(m,0)N_0(\sigma,k)\right]\right)F-H_2\left(\left[2\sum_{m=0}^{\infty}D_{\mathrm{II}}(m,0)N_0(\sigma,k)\right]^2+\left[2\sum_{m=0}^{\infty}D_{\mathrm{I}}(m,0)N_0(\sigma,k)\right]^2\right)F\\&-H_1\left[-2\sum_{m=0}^{\infty}D_{\mathrm{I}}(m,0)N_1(\sigma,k)\right]^2+4H_1\left(\left[\sum_{m=0}^{\infty}D_{\mathrm{II}}(m,0)N_0(\sigma,k)\right]\left[\sum_{m=0}^{\infty}D_{\mathrm{II}}(m,0)N_1(\sigma,k)\right]\right.\\&\left.+\left[\sum_{m=0}^{\infty}D_{\mathrm{I}}(m,0)N_0(\sigma,k)\right]\left[\sum_{m=0}^{\infty}D_{\mathrm{I}}(m,0)N_1(\sigma,k)\right]\right)G+4H_2\left(\left[\sum_{m=0}^{\infty}D_{\mathrm{II}}(m,0)N_1(\sigma,k)\right]\left[\sum_{m=0}^{\infty}D_{\mathrm{II}}(m,0)N_0(\sigma,k)\right]\right.\\&\left.+\left[\sum_{m=0}^{\infty}D_{\mathrm{I}}(m,0)N_1(\sigma,k)\right]\left[\sum_{m=0}^{\infty}D_{\mathrm{I}}(m,0)N_0(\sigma,k)\right]\right)G-4H_2\left(\left[\sum_{m=0}^{\infty}D_{\mathrm{I}}(m,0)N_1(\sigma,k)\right]\left[\sum_{m=0}^{\infty}D_{\mathrm{II}}(m,0)N_0(\sigma,k)\right]\right.\\&\left.-\left[\sum_{m=0}^{\infty}D_{\mathrm{II}}(m,0)N_1(\sigma,k)\right]\left[\sum_{m=0}^{\infty}D_{\mathrm{I}}(m,0)N_0(\sigma,k)\right]\right)+2H_3\left(\left\langle-4\left[\sum_{m=0}^{\infty}D_{\mathrm{I}}(m,t)kJ_1(k)\right]\left[\sum_{m=0}^{\infty}D_{\mathrm{II}}(m,t)kJ_0(k)\right]\right\rangle\right.\\&\left.-\sigma\left\langle-4\left[\sum_{m=0}^{\infty}D_{\mathrm{I}}(m,t)kJ_1(k)\right]\left[\sum_{m=0}^{\infty}D_{\mathrm{II}}(m,t)J_0(k)\right]\right\rangle\right)+2H_3\left(\sigma^2\left\langle-4\left[\sum_{m=0}^{\infty}D_{\mathrm{I}}(m,t)J_1(k)\right]\left[\sum_{m=0}^{\infty}D_{\mathrm{II}}(m,t)J_0(k)\right]\right\rangle\right.\\&\left.-\sigma\left\langle-4\left[\sum_{m=0}^{\infty}D_{\mathrm{I}}(m,t)J_1(k)\right]\left[\sum_{m=0}^{\infty}D_{\mathrm{II}}(m,t)kJ_0(k)\right]\right\rangle\right)-2H_4\sigma\left\langle-4\left[\sum_{m=0}^{\infty}D_{\mathrm{I}}(m,t)J_1(k)\right]\left[\sum_{m=0}^{\infty}D_{\mathrm{II}}(m,t)kJ_0(k)\right]\right\rangle\\&-H_1\left[2\sum_{m=0}^{\infty}D_{\mathrm{II}}(m,0)N_1(\sigma,k)\right]^2\Bigg\}\end{aligned}\tag{58}$$

where N_0 and N_1 are defined [10] as

https://doi.org/10.1017/jmech.2017.66 Published online by Cambridge University Press

$$N_0(\sigma,k)=(\sigma-k)J_0(k),\quad N_1(\sigma,k)=(\sigma-k)J_1(k). \tag{59}$$

From Eqs. (41), (56) and (58), the average power input coefficient can be obtained using

$$\langle P\rangle = U\langle T\rangle + \langle E_W\rangle. \tag{60}$$

4. THE FLEXIBLE PLATE WITH LINEAR AMPLITUDE AND DYNAMIC GROUND EFFECT

Equations (56), (58) and (60) give $\langle T\rangle$, $\langle E_W\rangle$ and $\langle P\rangle$, respectively in the general case in which the plate exhibits harmonic motion with arbitrary varying amplitude. As an example, the swimming performance of such a plate is studied in the case in which the plate is performing harmonic motion with linearly varying amplitude, and its swimming performance is determined from the thrust coefficient C_T, the power input coefficient C_P, the energy consumed per unit distance coefficient E_C, and the efficiency of propulsion η. Consider plate motion that is described by the equation

$$h(x,t)=\mathrm{Re}\left[\left(b_0+b_1xe^{j\varepsilon}\right)e^{j(\omega t-kx)}\right]=b_0\cos(\omega t-kx)+b_1x\cos(\omega t-kx+\varepsilon), \tag{61}$$

A comparison with Eq. (50) yields $b_2=b_3=\ldots=0$, $\varepsilon_0=0$, and $\varepsilon_1=\varepsilon$.

Substituting m from Eq. (61) into Eq. (51) and substituting Eqs. (51), (53), and (57) into Eq. (56) straightforwardly yields

$$\begin{aligned}C_T=\frac{\langle T\rangle}{\pi\rho U^2}&=b_0^2\left[T_1(\sigma,k)+T_5(\sigma,k)\right]+b_1^2\left[T_2(\sigma,k)+T_6(\sigma,k)\right]\\&+b_0b_1\left[\left(T_3(\sigma,k)+T_7(\sigma,k)\right)\cos\varepsilon+\left(T_4(\sigma,k)+T_8(\sigma,k)\right)\sin\varepsilon\right],\end{aligned} \tag{62}$$

where C_T was separated into eight components that are given by

$$\begin{aligned}&T_1(\sigma,k)=\Omega(\sigma,k)\Omega_*(\sigma,k)+Q(\sigma,k)Q_*(\sigma,k),\quad T_2(\sigma,k)=\frac{\partial\Omega}{\partial k}\frac{\partial\Omega_*}{\partial k}+\frac{\partial Q}{\partial k}\frac{\partial Q_*}{\partial k},\\&T_3(\sigma,k)=Q\frac{\partial\Omega}{\partial k}+Q_*\frac{\partial\Omega_*}{\partial k}-\Omega\frac{\partial Q}{\partial k}-\Omega_*\frac{\partial Q_*}{\partial k}+\sigma^2\left[J_0^2+J_1^2-\frac{1}{k}J_0J_1\right],\quad T_4(\sigma,k)=-\frac{\partial T_1(\sigma,k)}{\partial k},\\&T_5(\sigma,k)=-H_1Q_1(\sigma,k)-H_2\Omega_2(\sigma,k),\quad T_6(\sigma,k)=-H_1Q_3(\sigma,k)-H_2\Omega_4(\sigma,k),\\&T_7(\sigma,k)=H_1\Omega_1(\sigma,k)-H_2Q_4(\sigma,k)+H_3K_1+\frac{\sigma^2}{2}H_3K_2-2\sigma H_3K_3,\\&T_8(\sigma,k)=H_1Q_2(\sigma,k)+H_2\Omega_3(\sigma,k).\end{aligned} \tag{63}$$

where the functions $J_n(k)$ in Eq. (63) are Bessel functions of the first kind, and expressions for Ω, Q, Q_* and Ω_* are obtained from Eqs. (53) and (57). The other functions in Eq. (63) which are Q_n and Ω_n (for $n=1,2,3,4$), and K_m (for $m=1,2,3$), are defined as

$$\begin{aligned}&Q_1(\sigma,k)\equiv Q(\sigma,k)kJ_1(k),\quad Q_2(\sigma,k)\equiv Q(\sigma,k)\frac{\partial kJ_1(k)}{\partial k}+kJ_1(k)\frac{\partial Q(\sigma,k)}{\partial k},\\&Q_3(\sigma,k)\equiv\left(\frac{\partial Q(\sigma,k)}{\partial k}\right)\left(\frac{\partial kJ_1(k)}{\partial k}\right),\quad Q_4(\sigma,k)\equiv Q(\sigma,k)\frac{\partial kJ_0(k)}{\partial k}-kJ_0(k)\frac{\partial Q(\sigma,k)}{\partial k},\\&\Omega_1(\sigma,k)\equiv\Omega(\sigma,k)\frac{\partial kJ_1(k)}{\partial k}-kJ_1(k)\frac{\partial\Omega(\sigma,k)}{\partial k},\quad K_1\equiv kJ_1(k)\frac{\partial kJ_0(k)}{\partial k}-kJ_0(k)\frac{\partial kJ_1(k)}{\partial k},\\&\Omega_3(\sigma,k)\equiv\Omega(\sigma,k)\frac{\partial kJ_0(k)}{\partial k}+kJ_0(k)\frac{\partial\Omega(\sigma,k)}{\partial k},\quad \Omega_4(\sigma,k)\equiv\left(\frac{\partial\Omega(\sigma,k)}{\partial k}\right)\left(\frac{\partial kJ_0(k)}{\partial k}\right),\\&\Omega_2(\sigma,k)\equiv\Omega(\sigma,k)kJ_0(k),\quad K_2\equiv J_0(k)\frac{\partial kJ_0(k)}{\partial k}-kJ_0(k)\frac{\partial J_0(k)}{\partial k},\\&K_3\equiv J_1(k)\frac{\partial kJ_0(k)}{\partial k}-kJ_0(k)\frac{\partial J_1(k)}{\partial k}.\end{aligned} \tag{64}$$

In a manner similar to that in which Eq. (62) was obtained, Eq. (58) becomes

https://doi.org/10.1017/jmech.2017.66 Published online by Cambridge University Press

$$\frac{\langle E_W \rangle}{\pi\rho U^3} = b_0^2\left[W_1(\sigma,k)+W_5(\sigma,k)\right]+b_1^2\left[W_2(\sigma,k)+W_6(\sigma,k)\right]$$
$$+b_0b_1\left[\left(W_3(\sigma,k)+W_7(\sigma,k)\right)\cos\varepsilon+\left(W_4(\sigma,k)+W_8(\sigma,k)\right)\sin\varepsilon\right], \tag{65}$$

which was also separated into eight components that are given by

$$W_1(\sigma,k)=\left[F-\left(F^2+G^2\right)\right]\left[N_0^2+N_1^2\right],\quad W_2(\sigma,k)=\left[F-\left(F^2+G^2\right)\right]\left[\left(\frac{\partial N_0}{\partial k}\right)^2+\left(\frac{\partial N_1}{\partial k}\right)^2\right],$$
$$W_3(\sigma,k)=2\left[F-\left(F^2+G^2\right)\right]\left[N_0\frac{\partial N_1}{\partial k}-N_1\frac{\partial N_0}{\partial k}\right],\quad W_4(\sigma,k)=-\frac{\partial W_1(\sigma,k)}{\partial k},$$
$$W_5(\sigma,k)=\left(H_1N_1^2-H_2N_0^2\right)F+\left(H_1+H_2\right)N_0N_1G-H_1N_1^2,$$
$$W_6(\sigma,k)=\left\{\left[H_1\left(\frac{\partial N_1}{\partial k}\right)^2-H_2\left(\frac{\partial N_0}{\partial k}\right)^2\right]F+\left(H_1+H_2\right)\left(\frac{\partial N_0}{\partial k}\right)\left(\frac{\partial N_1}{\partial k}\right)G-H_1\left(\frac{\partial N_1}{\partial k}\right)^2\right\},$$
$$W_7(\sigma,k)=\left\{\left(N_0\frac{\partial N_1}{\partial k}-N_1\frac{\partial N_0}{\partial k}\right)F\left(H_1-H_2\right)+H_2\left(N_0\frac{\partial N_1}{\partial k}-N_1\frac{\partial N_0}{\partial k}\right)-H_3K_1\right.$$
$$\left.+\sigma\left(H_3K_4+H_4K_3+H_3K_3\right)-\sigma^2H_3K_5\right\},$$
$$W_8(\sigma,k)=\left\{\left(H_2N_0\frac{\partial N_0}{\partial k}-H_1N_1\frac{\partial N_1}{\partial k}\right)2F-\left(N_0\frac{\partial N_1}{\partial k}+N_1\frac{\partial N_0}{\partial k}\right)G\left(H_1+H_2\right)+2H_1N_1\frac{\partial N_1}{\partial k}\right\}, \tag{66}$$

where the functions N_0 and N_1 are defined in Eq. (59), and the functions K_1 and K_3 are defined in Eq. (64). The functions K_4 and K_5 are defined as

$$K_4\equiv kJ_1(k)\frac{\partial J_0(k)}{\partial k}-J_0(k)\frac{\partial kJ_1(k)}{\partial k},\quad K_5\equiv J_1(k)\frac{\partial J_0(k)}{\partial k}-J_0(k)\frac{\partial J_1(k)}{\partial k}. \tag{67}$$

The average power input coefficient can be obtained straightforwardly from Eqs. (60), (62) and (65), such that it can also be separated into eight components as

$$C_p=\frac{\langle P\rangle}{\pi\rho U^3}=b_0^2\left[P_1(\sigma,k)+P_5(\sigma,k)\right]+b_1^2\left[P_2(\sigma,k)+P_6(\sigma,k)\right]$$
$$+b_0b_1\left[\left(P_3(\sigma,k)+P_7(\sigma,k)\right)\cos\varepsilon+\left(P_4(\sigma,k)+P_8(\sigma,k)\right)\sin\varepsilon\right], \tag{68}$$

with

$$P_m(\sigma,k)=T_m(\sigma,k)+W_m(\sigma,k),\ \text{for}\ m=1,2,3,...,8. \tag{69}$$

Finally, the average efficiency of propulsion is defined as

$$\eta=\frac{U\langle T\rangle}{\langle P\rangle}=\frac{C_T}{C_P}. \tag{70}$$

The energy consumed per unit distance, which is the energy required to travel one body length, is defined [11] as

$$E_C=\frac{C_P}{\sigma^2}. \tag{71}$$

Equations (62), (68), (70) and (71) respectively represent the thrust coefficient, the power input coefficient, the efficiency and the coefficient of the energy consumed per unit distance for a swimming plate under the dynamic ground effect, whose waving motion is a linearly varying amplitude harmonic motion.

5. RESULTS

The equations for C_T, C_P, η and E_C that appeared in the preceding section are all functions of the distance h' between the plate and the wall. If distance h' is sufficiently large, then the effect of the wall on the swimming performance of the plate can be neglected. Therefore, as $h'\to\infty$ expressions associated with the unbounded fluid, are obtained for the thrust, the power input, the energy loss, the efficiency and the energy consumed per unit distance. Hence,

https://doi.org/10.1017/jmech.2017.66 Published online by Cambridge University Press

$$\lim_{h'\to\infty}\frac{\langle T\rangle}{\pi\rho U^2}=\left[\frac{\langle T\rangle}{\pi\rho U^2}\right]_{Unbounded},\quad \lim_{h'\to\infty}\frac{\langle E_W\rangle}{\pi\rho U^3}=\left[\frac{\langle E_W\rangle}{\pi\rho U^3}\right]_{Unbounded},\quad \lim_{h'\to\infty}\frac{\langle P\rangle}{\pi\rho U^3}=\left[\frac{\langle P\rangle}{\pi\rho U^3}\right]_{Unbounded},$$

$$\lim_{h'\to\infty}\eta=[\eta]_{Unbounded},\quad \lim_{h'\to\infty}E_C=[E_C]_{Unbounded}, \tag{72}$$

where the subscript "unbounded" indicates that the results obtained are for a situation in which the plate is swimming in the absence of a dynamic ground effect (without a wall).

To analyze the swimming performance of the plate under the dynamic ground effect, the analytical model that is proposed in this study is applied to a situation in which the undulating plate with linearly changing amplitude is swimming close to, and far from, a planar wall. The following table provides the kinematic parameters of the plate.

Table 1 Kinematic parameters of undulating plate that swims in the presence of a planar wall, with distance between plate and wall given in body lengths (B.L)

Amplitude	Amplitude Coefficients (61)	Wave number	Distance to wall (B.L)	Reduced frequency	Wall Condition (B.L)	
					Near	Far
Linear	$b_0 = 1.21$, $b_1 = 0.12$	$k = 1\times10^{-5}$, 0.1, 0.278, 0.4, 0.7, 1	$0 \le h' \le 1$	$0 \le \sigma \le 10$	$h' = 0.3$	$h' = 1$

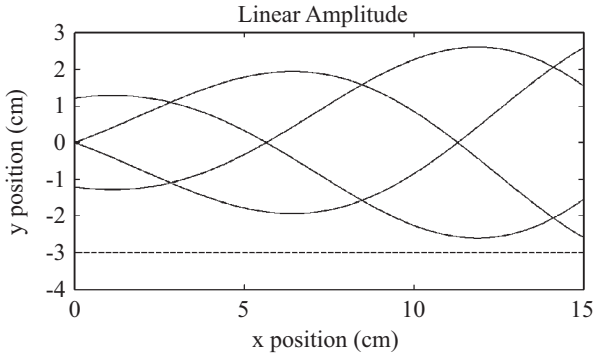


Fig. 2 Swimming motion of plate with linearly varying amplitude of oscillation and $k \cong 0.278$. Each trace represents one quarter of the plate's motion during one cycle of oscillation. Dashed line represents a wall.

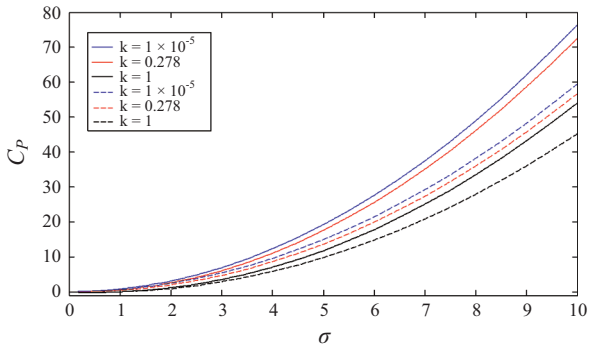


Fig. 3 Power coefficient C_P plotted against reduced frequency σ, for a plate that is swimming close to a wall at $h' = 0.3$ B.L. (dashed lines), and far from a wall at $h' = 1$ B.L (solid lines).

E. Blevins and G. V. Lauder [1] performed experimental studies to analyze the effect of a planar wall on the locomotion of a robotic fin that exhibits undulating motion. The amplitude and wave number parameters from Table 1 were obtained by estimating the kinematic parameters of the robotic fin that was used in Ref. [1], such that the midline traces through time of the plate which are presented in Fig. 2 herein, resemble those of the robotic fin from Fig. 3 in the work of E. Blevins and G. V. Lauder [1].

The following results were obtained by applying the kinematic conditions from Table 1 to the results in section 4. The swimming performance of a plate that oscillates with a linearly varying amplitude under the dynamic ground effect.

Figure 3 reveals that the dynamic ground effect reduced the power input of the plate, as is observed by comparing the behaviors of C_P under near (dashed lines) and far (solid lines) wall conditions for each value of k. Figure 4 shows that the effect of the wall was to slightly

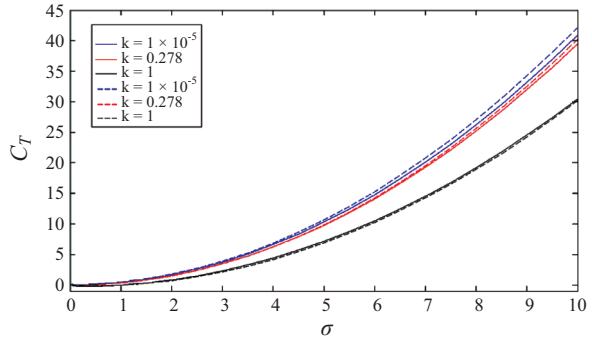


Fig. 4 Thrust coefficient C_T plotted against reduced frequency σ, for a plate that is swimming close to a wall at $h' = 0.3$ B.L. (dashed lines), and far from a wall at $h' = 1$ B.L (solid lines).

change the thrust, as observed by comparing the behaviors of C_T under near (dashed lines) and far (solid lines)

https://doi.org/10.1017/jmech.2017.66 Published online by Cambridge University Press

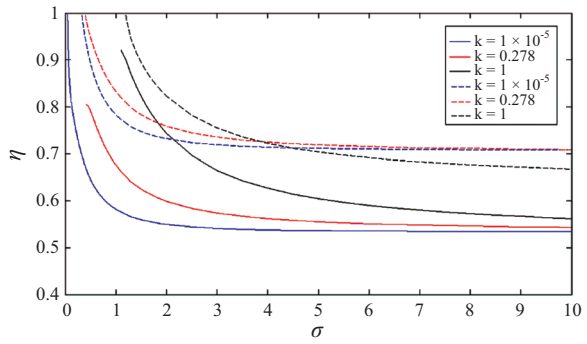


Fig. 5 Efficiency η plotted against reduced frequency σ, for a plate that is swimming close to a wall at h' = 0.3 B.L. (dashed lines), and far from a wall at h' = 1 B.L (solid lines).

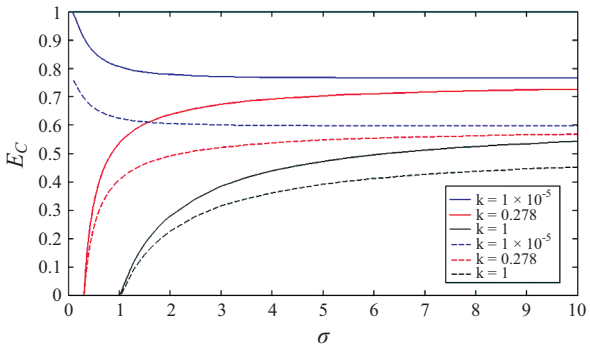


Fig. 6 Energy consumed per unit distance E_C plotted against reduced frequency σ, for a plate that is swimming close to a wall at h' = 0.3 B.L. (dashed lines), and far from a wall at h' = 1 B.L (solid lines).

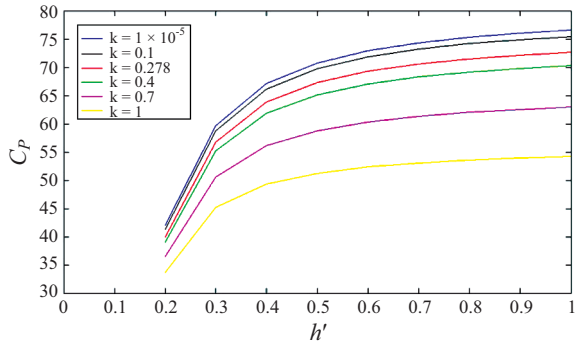


Fig. 7 Power coefficient C_P versus distance h' between plate and wall for various values of k and σ = 10.

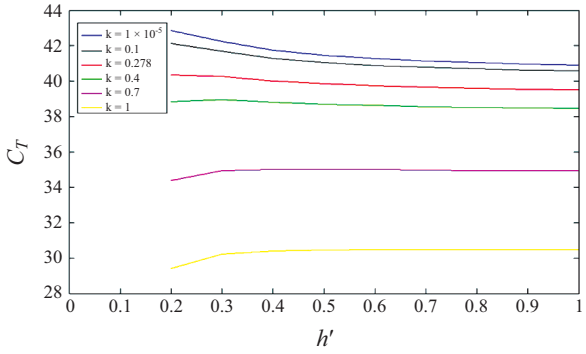


Fig. 8 Thrust coefficient C_T versus distance h' between plate and wall for various values of k and σ = 10.

wall conditions for each value of k. Notably, C_T was slightly higher for small values of k ($k = 1 \times 10^{-5}$ & k = 0.278) when the plate was swimming close to the wall (dashed lines) than when it was swimming far from it (solid lines). But C_T was slightly lower at a larger value of k (k = 1) when the plate was swimming close to the wall (dashed lines) than when it was swimming far from it (solid lines). This change in the behavior of C_T with σ for different values of k suggests that the impact of the dynamic ground effect depended on the kinematic conditions of the plate. Additionally, qualitatively comparing Figs. 3 and 4 reveals that when the plate was swimming close to the wall, C_P was reduced by more than did C_T. Therefore, the swimming performance of the plate was improved by the substantial reduction of the power input while the thrust was kept almost constant, so the difference in thrust between near and far wall conditions was small. Therefore, when the plate was swimming near the wall, it produced almost the same thrust as when it was swimming far from the wall, but with less power input required to maintain its undulating motion. These behaviors of C_T and C_P when the plate was swimming close to the wall positively influenced the efficiency of propulsion η, so η increased as expected from its definition in (70). This finding is evident in Fig. 5, in which the efficiency of the plate when it was swimming close to the wall (dashed lines) exceeded that when it was swimming far from the wall (solid lines). Finally, the coefficient of energy consumption per unit distance of the plate, E_C, was lower for each value of k when the plate was swimming close to the wall than when it was swimming farther from it, as can be shown in Fig. 6. This result is expected from the definition of E_C in Eq. (71), in which E_C and C_P are directly proportional to each other, such that when the plate requires less power input, it consumes less energy.

Figures 7 and 10 show that as h' decreased, C_P and E_C decreased. However, from Fig. 8 as h' decreased, C_T increased or decreased depending on the value of k, such that for small values of h', C_T increased (decreased) as k decreased (increased). In spite of the change of C_T at small h', the changes in C_T (Fig. 8) were smaller than those in C_P (Fig. 7); therefore η increased as h' decreased, as presented in Fig. 9. Therefore, the dynamic ground effect on the plate improved its swimming performance by greatly reducing the power input while maintaining an almost constant thrust; thus the efficiency of propulsion was increased and the energy consumption per unit dis-

https://doi.org/10.1017/jmech.2017.66 Published online by Cambridge University Press

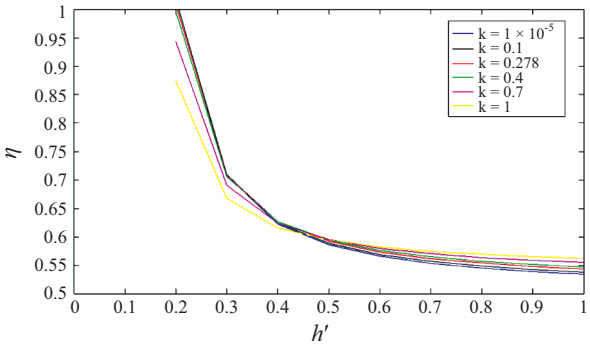


Fig. 9 Efficiency η versus distance h' between plate and wall for various values of k and $\sigma = 10$.

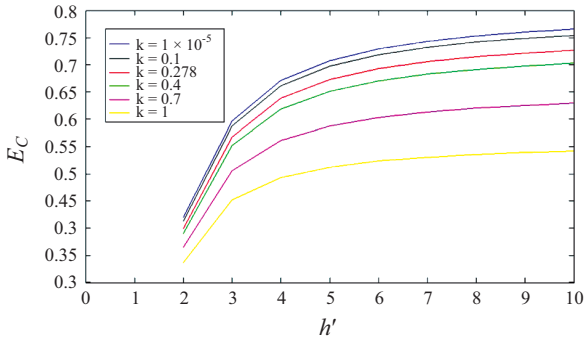


Fig. 10 Energy consumed per unit distance E_C versus distance h' between plate and wall for various values of k and $\sigma = 10$.

tance was reduced, as observed in Figs. 3-10.

As observed in Fig. 9, no single preferred distance between the plate and the wall existed at which the efficiency was maximized under all kinematic conditions of the plate. Rather, the distance to the wall at which the efficiency of the plate was maximized depended on the kinematic conditions of the plate: a range of h' existed in which the plate exhibited the highest possible efficiency for all the considered wave numbers k. In the example that was considered in this study, under the kinematic conditions from Table 1, the range of h' in which the plate achieved the highest efficiency was $0.2 \leq h' \leq 0.3$ B.L.

6. CONCLUSIONS

This work contributes an analytical model of the dynamic ground effect, whose results agree qualitatively with experimental results [1,2] in that the degree of impact of the dynamic ground effect on the swimming performance of a plate depended on its kinematic conditions. As an example, this model was used to study the swimming performance of a plate with a linearly varying amplitude of oscillation. General expressions for the thrust coefficient, power input coefficient, propulsive efficiency and energy consumption (C_T, C_P, η and E_C, respectively) of the plate were obtained and analyzed in two situations when the plate was swimming near and far from the wall. Each situation was analyzed under the various kinematic conditions that appear in Table 1.

The presence of a nearby wall enhanced the swimming performance of the plate above that achieved when the plate is far from a wall. This enhancement arose from a large reduction in the required power input (C_P), which in turn reduced the energy consumed by the plate (E_C). Meanwhile, the thrust coefficient (C_T) was slightly reduced or increased, depending on the wave number k and distance from the wall h'. Comparing the changes in the power input and thrust coefficients that were induced by the wall reveals that the dynamic ground effect substantially reduced the power input while without significantly changing the thrust, increasing the propulsive efficiency of the plate. However, the magnitude of the dynamic ground effect on the swimming performance of the plate depended on the kinematic conditions of the plate.

The range of distances h' between the plate and the wall in which the efficiency of the propulsion of the plate was maximized depended on the value of k, which is the wave number of the plate. Therefore, no single distance from the wall optimized swimming performance under all kinematic conditions, owing to the dynamic ground effect. Instead, a range of distances between the plate and the wall existed for which the wall provided hydrodynamic assistance to the plate, but the magnitude of this assistance depended on the kinematic conditions of the plate.

Recently, the field of biologically inspired underwater vehicles such as BAUV's (Biomimetic Autonomous Underwater Vehicles) has seen significant growth. Despite current applications of, and research done on, biologically inspired manmade devices, gaps in understanding limit their application. Therefore, this work may provide a useful theoretical starting point to filling these gaps, which concerns the dynamic ground effect. Following this work, BAUV's may be designed in to exploit hydrodynamically the dynamic ground effect. For example, this work may be useful in understanding and predicting the kinematic conditions under which a BAUV can perform wall tracking tasks and move close to ground or a substrate in manner that saves energy without loss of propulsive efficiency.

As it has been reported elsewhere [1, 2], fish modify their kinematic conditions when swimming close to a substrate. Therefore, although the proposed model of the dynamic ground effect is simplified and rests on many assumptions regarding linearity and viscosity to yield a closed-form analytical solution, it can be used to predict and analyze the impact of the dynamic ground effect on the swimming performance of flat fish (such as stingrays) under various kinematic conditions.

AKNOWLEDGEMENTS

The authors would like to thank the National Museum of Science and Technology (Contract No. S102-03-05),

https://doi.org/10.1017/jmech.2017.66 Published online by Cambridge University Press

and the National Science Council of the Republic of China, Taiwan (Contract No. NSC101-2221-E-002-119) for the financial support of this research.

REFERENCES

1. Blevins, E. and Lauder, G. V., "Swimming Near the Substrate: A Simple Robotic Model of Stingray Locomotion," *Bioinspiration & Biomimetics*, **8**, 016005 (2013).
2. Webb, P. W., "Kinematics of Plaice, *Pleuronectes platessa*, and Cod, *Gadus morhua*, Swimming Near the Bottom," *Journal of Experimental Biology*, **205**, pp. 2125-2134 (2002).
3. Kanso, E. and Newton, P. K., "Locomotory Advantages to Flapping Out of Phase," *Experimental Mechanics,* **50**, pp. 1367-1372 (2010).
4. Nowroozi, B. N., Strother, J. A., Horton, J. M., Summers, A. P. and Brainerd, E. L., "Whole-Body Lift and Ground Effect During Pectoral Fin Locomotion in the Northern Spearnose Poacher (*Agonopsis vulsa*)," *Zoology,* **112**, pp. 393-402 (2009).
5. Prats, R. F., Raspa, V., Thiria, B., Huarte, F. H. and Diana, R. G., "Large-Amplitude Undulatory Swimming Near a Wall," *Bioinspiration & Biomimetics*, **10**, pp. 1-15 (2015).
6. Quinn, D. B., Moored, K. W., Dewey, P. A. and Smits, A. J., "Unsteady Propulsion Near a Solid Boundary," *Journal of Fluid Mechanics*, **742**, pp. 152-170 (2014).
7. Quinn, D. B., Lauder, G. V. and Smits, A. J., "Flexible Propulsors in Ground Effect," *Bioinspiration & Biomimetics*, **9**, 036008 (2014).
8. Dai, L. Z., He, G. W. and Zhang, X., "Self-Propulsion of a Flexible Plunging Foil Near a Solid Wall," *Proceedings of the 7 th International Conference on Fluid Mechanics ICFM7, Procedia Engineering*, Beijing, China, **126**, pp. 431-435 (2015).
9. Fung, Y. C., *An Introduction to the Theory of Aeroelasticity*, Dover Publications, Inc., New York, (2008).
10. Wu, Y. T., "Swimming of a Waving Plate," *Journal of Fluid Mechanics*, **10**, pp. 321-344 (1961).
11. Eloy, C. and Schouveiler, L., "Optimization of Two-Dimensional Undulatory Swimming at High Reynolds Number," *International Journal of Non-Linear Mechanics*, **46**, pp. 568-576 (2011).
12. Luke, Y. L. and Dengler, M. A., "Tables of the Theodorsen Circulation Function for Generealized Motion," *Journal of the Aeronautical Sciences*, **18**, pp. 478-483 (1951).
13. Schlichting, H. and Gersten, K., *Boundary-Layer Theory*, Springer-Verlag, Berlin (2003).

(Manuscript received October 12, 2016,
accepted for publication July 14, 2017.)

https://doi.org/10.1017/jmech.2017.66 Published online by Cambridge University Press